J Appl Electrochem (2012) 42:463–470
DOI 10.1007/s10800-012-0424-2

ORIGINAL PAPER

Electrochemical properties of microwave-assisted reflux-synthesized Mn_3O_4 nanoparticles in different electrolytes for supercapacitor applications

Kalimuthu Vijaya Sankar · D. Kalpana · Ramakrishnan Kalai Selvan

Received: 15 March 2012 / Accepted: 26 April 2012 / Published online: 11 May 2012

Abstract The nanosized Mn_3O_4 particles were prepared by microwave-assisted reflux synthesis method. The prepared sample was characterized using various techniques such as X-ray diffraction (XRD), Fourier transform-infrared spectroscopy (FT-IR), Raman analysis, and transmission electron microscopy (TEM). Electrochemical properties of Mn_3O_4 nanoparticles were investigated using cyclic voltammogram (CV), electrochemical impedance spectroscopy (EIS), and galvanostatic charge–discharge analysis in different electrolytes such as 1 M KCl, 1 M Na_2SO_4, 1 M $NaNO_3$, and 6 M KOH electrolytes. XRD pattern reveals the formation of single-phase Mn_3O_4 nanoparticles. The FT-IR and Raman analysis also assert the formation of Mn_3O_4 nanoparticles. The TEM image shows the spherical shape particles with less than 50 nm sizes. Among all the electrolytes, the Mn_3O_4 nanoparticles possess maximum specific capacitance of 94 F g^{-1} in 6 M KOH electrolyte calculated from CV. The order of capacitance obtained by various electrolytes is 6 M KOH > 1 M KCl > 1 M $NaNO_3$ > 1 M Na_2SO_4. The EIS and galvanostatic charge–discharge results further substantiate with the CV results. The cycling stability of Mn_3O_4 electrode reveals that the prepared Mn_3O_4 nanoparticles are a suitable electrode material for supercapacitor application.

K. V. Sankar · R. K. Selvan (✉)
Solid State Ionics and Energy Devices Laboratory, Department of Physics, Bharathiar University, Coimbatore 641 046, India
e-mail: selvankram@buc.edu.in

D. Kalpana
Electrochemical Power Systems Division, Central Electrochemical Research Institute, Karaikudi 630 006, Tamil Nadu, India

Keywords Mn_3O_4 · Microwave-assisted reflux · Nanoparticles · Electrolytes · Specific capacitance

1 Introduction

Recently, an enormous effort has been focused on the fabrication of electrochemical capacitors or supercapacitors for energy storage due to their long cycle life and higher power and energy density than batteries and conventional capacitors [1]. It is well known that the electrochemical capacitors can be classified into two types such as pseudocapacitor and electric double layer capacitors (EDLC) based on their energy storage mechanism. In pseudocapacitors, the energy is stored through oxidation/reduction or Faradaic reaction occurred at the electrode surface. The transition metal oxides and conducting polymer materials are widely used as electrode material for pseudocapacitors. Similarly in EDLC, the energy is stored at electrode/electrolyte interfaces via double layer formation. Carbon-based materials are widely used as EDLC electrodes due to their higher surface area [2]. There are various metal oxides synthesized for supercapacitor application such as RuO_2 [3], NiO [4], Co_3O_4 [5], Bi_2O_3 [6], SnO_2 [7], and manganese-based oxides [8–10]. Among all the transition metal oxides, RuO_2 possesses higher specific capacitance of 720 F g^{-1} [11]. However, it has been less considered due to their high cost, need of strong acidic electrolyte, and toxicity of the material [12, 13]. Hence, it is believed that the manganese oxide-based electrode materials can replace the RuO_2 for supercapacitor applications because of their low cost and environmental friendly nature [14] as well as its different crystallographic forms of MnO, Mn_3O_4, Mn_2O_3, and MnO_2 due to the existence of various oxidation states [15, 16].

Generally, the specific capacitance of the Mn_3O_4 mainly depends upon various parameters such as specific surface area [9], preparation conditions [17], synthesis method [16–29], active materials loading [30], morphology [31], conductive additives (carbon, CNT, Graphene) [32–34], electrolyte concentration [22], and potential window [30, 35]. Conventionally, the oxides (MnO_2, Mn_2O_3), carbonate ($MnCO_3$), nitrate ($Mn(NO_3)_2$), and sulfate ($MnSO_4$) salts of manganese are heated at above 1000 °C to form a Mn_3O_4 tetragonal structure [25, 36]. Subsequently, to improve the specific capacitance of Mn_3O_4, the nanosized particles have been prepared by various methods such as successive ionic layer adsorption and reaction (SILAR) [18], hydrothermal [17, 20], solution combustion [21], chemical bath deposition [22], oxidative precipitation [23], sonochemical [24], solvothermal [25], and microwave [26–29].

In this line, the main aim of this present work is to prepare Mn_3O_4 nanoparticles by microwave-assisted reflux synthesis with a very short reaction time (5 min) using low power of 20 W without further high-temperature calcinations and explored its application as electrodes for supercapacitors. To the best of our knowledge, there is no previous literature available on the synthesis of Mn_3O_4 nanoparticles using this procedure and optimization of electrolyte. In addition, here we have used ethylene glycol as a reactive medium for the microwave synthesis due to its high-dissipation factor (1.35) than other solvents such as water (0.157), formic acid (0.722) and so on. Further the prepared sample was characterized by X-ray diffraction (XRD), Fourier transform-infrared spectroscopy (FT-IR), laser Raman spectra, scanning electron microscopy (SEM), and transmission electron microscopy (TEM). The electrochemical performance of Mn_3O_4 was investigated using cyclic voltammetry, electrochemical impedance, spectroscopic, and galvanostatic charge–discharge analysis in various aqueous electrolytes such as 1 M Na_2SO_4, 1 M $NaNO_3$, 1 M KCl, and 6 M KOH for optimizing the suitable electrolyte for Mn_3O_4 electrode in supercapacitor applications. The results indicate that the obtained nanosphere Mn_3O_4 is a good electrode material for supercapacitor application.

2 Experimental methods and materials

All the chemicals used were of analytical grade and used without any further purification. Manganese chloride tetrahydrate ($MnCl_2{\cdot}4H_2O$) and sodium hydroxide (NaOH) were purchased from Himedia. Ethylene glycol was purchased from Merck. The stoichiometric amounts of $MnCl_2{\cdot}4H_2O$ were dissolved in distilled water with EG (50 ml), and NaOH solution was added drop by drop under vigorous stirring. The color of the solution changed in to brown color precipitate. This precipitate was placed in microwave irradiation (Domestic microwave oven, LG) for refluxing with power of 20 W, the ON/OFF cycle duration as 15 s/15 s, with the total reaction time of 5 min [37, 38]. The ON/OFF cycle was used to control the overheating. Finally, the as-prepared sample was centrifuged several times in double distilled water, ethanol, and dried at 100 °C overnight.

The phase purity and compound formation were characterized by an X-ray diffractometer, Bruker D8 Advance with Cu Kα radiation. The morphology of the as-prepared samples was found using TEM analysis (JEOL model JEM 2011 at an accelerating voltage of 200 kV). The functional groups were identified using FT-IR Perkin Elmer make model RXI instrument. The Raman analysis of our samples was carried out in the instrument of laser Raman confocal microprobe (Lab Ram HR 800). He–Ne laser ($\lambda = 633$ nm) was used as the excitation source with output power of 17 mW which was focused on to a spot of 1 μm. The cyclic voltammetrics analysis was carried out in CHI 1102A electrochemical workstation. The galvanostatic charge–discharge analysis was carried in Biologic SP-150 electrochemical workstation.

The Mn_3O_4 active material, carbon black, and PVdF were taken in the weight ratio of 80:15:5. All these were mixed together using NMP (N-methylpyrrolidone) as a solvent. The detailed electrode preparation is given elsewhere [39]. The electrochemical analysis was carried out in three-electrode configuration with Mn_3O_4-coated graphite sheet, Pt and SCE, Ag/AgCl as working, counter, and reference electrodes, respectively. Here we used different electrolytes such as 1 M Na_2SO_4, 6 M KOH, 1 M $NaNO_3$, and 1 M KCl to optimize the suitable electrolyte for Mn_3O_4 electrode material for supercapacitor application.

3 Results and discussion

3.1 Structural and morphological properties

The XRD pattern of Mn_3O_4 nanoparticles is given in Fig. 1. All the diffraction peaks were indexed to the tetragonal structure (space group $I41/amd$). No other impurity peaks were found, which reveals the phase purity of the prepared sample. However, the observed broadened and low-intensity peaks indicate the less crystallinity of the as-prepared Mn_3O_4 nanoparticles. The lattice parameters ($a = b = 5.767$ Å and $c = 9.485$ Å), lattice density (4.816 g cm^{-3}), and cell volume (315.5 $Å^3$) of the sample were calculated which are in good consistence with JCPDS data (card no. 89-4837). The crystallite size was calculated using Debye–Scherrer formula, and the average crystallite size is 18 nm, which is less than the reported value [40]. The surface area of the as-prepared Mn_3O_4

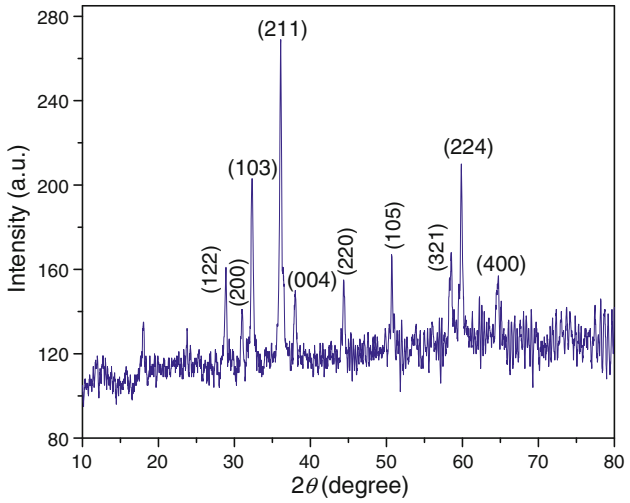

Fig. 1 XRD pattern of the Mn_3O_4 sample

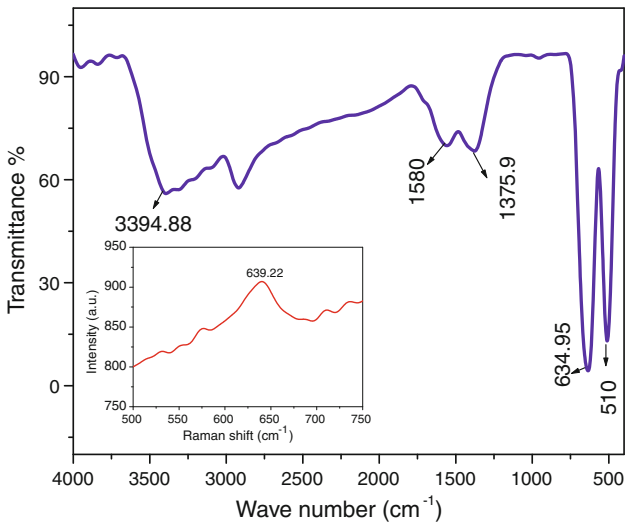

Fig. 2 FT-IR spectrum of the Mn_3O_4 sample and *inset* is Raman spectrum of Mn_3O_4 sample

nanoparticles was theoretically calculated [41], and the value is 65 m^2 g^{-1}.

The FT-IR spectrum of Mn_3O_4 (Fig. 2) shows two significant peaks at 635 and 510 cm^{-1}, which corresponds to the coupling between the Mn–O stretching modes of tetrahedral and octahedral sites, respectively. In addition, a broad peak was observed around 3395 cm^{-1} indicating the presence of –OH group. Further, the small band was observed around 1580 cm^{-1} corresponding to the adsorption of moisture on the surface of the sample, and also a small peak was observed around 1376 cm^{-1} corresponding to the bending vibration of O–H bonds connected with Mn atoms [35]. The presence of Mn–O stretching modes and water content was identified through the FT-IR study. Similarly, the characteristic Raman peak of Mn_3O_4 spinel

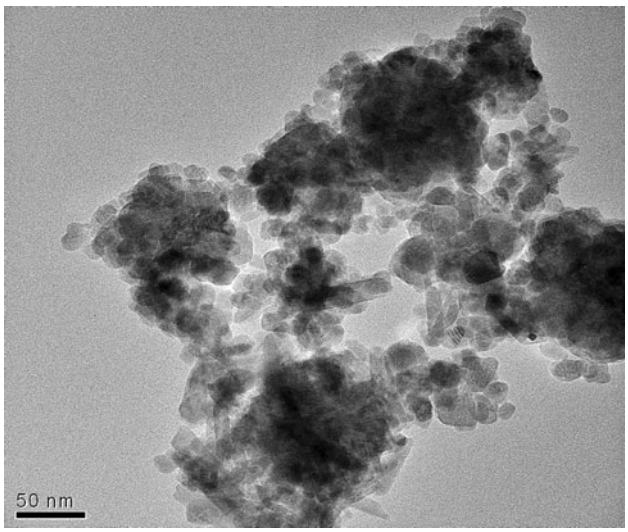

Fig. 3 TEM image of the Mn_3O_4 sample

(Fig. 2 inset) was obtained at 639 cm^{-1}, which is comparable with the reported values of 658.4 and 658 cm^{-1} [25, 42]. The observed peak broadening reveals the smaller crystallite size as well as the low crystallinity of Mn_3O_4 nanoparticles [43]. Because of their smaller crystallite size, the material has high uncertainty of momentum which leads to the broadening of the Raman peak [43].

The TEM image of Mn_3O_4 (Fig. 3) shows the formation of individual spherical nanoparticles with uniform size of less than 50 nm. It can also be seen that some partial aggregation of nanospheres. This aggregation of nanoparticles may be due to the effect of microwave heating. That is, it creates "hot surface" on the initially produced nanoparticles which leads to the particle aggregation. Because of the smaller particle size, it may provide higher surface area which may enhance the electrochemical reaction.

3.2 Electrochemical properties

3.2.1 Cyclic voltammogram analysis

Figure 4a–d shows the cyclic voltammogram (CV) curves of Mn_3O_4 in different electrolytes (1 M Na_2SO_4, 6 M KOH, 1 M $NaNO_3$, and 1 M KCl) at different scan rates of 5, 10, 20, 30, 40, 50, and 100 mV s^{-1}. The more or less rectangular shape of the voltammogram reveals the capacitive behavior of Mn_3O_4. It can be seen that the current under curve increases with increase in scan rate and in turn results in decrease in capacitance (Fig. 4e). It is well known that the voltammetric current is always directly proportional to the scan rate [7]. At low-scan rate, the ions from the electrolyte can utilize all the available sites in the active electrode material, because the ions have enough

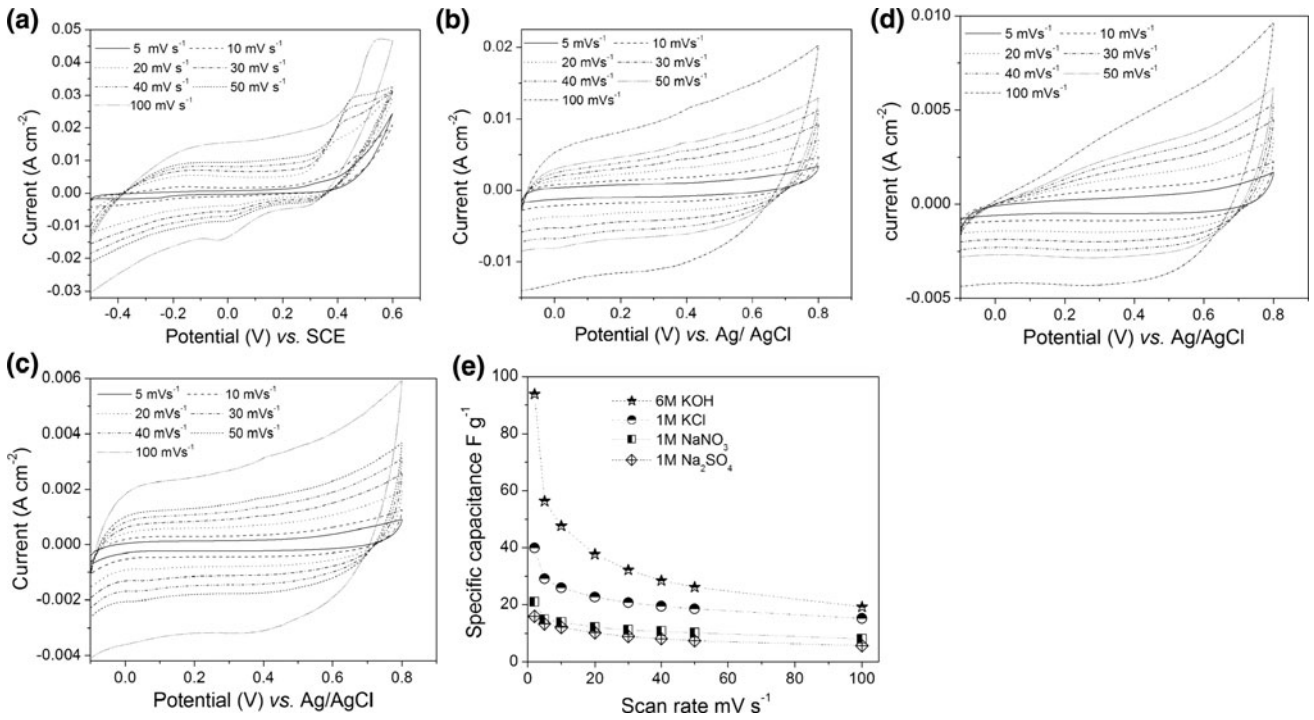

Fig. 4 CV curve of Mn_3O_4 electrode in **a** 6 M KOH, **b** 1 M KCl, **c** 1 M $NaNO_3$ **d** 1 M Na_2SO_4, and **e** variation of specific capacitance with scan rate

time to diffuse into all the sites which leads to the higher capacitance. On the other hand, at high-scan rate, the ions from electrolyte confront the difficulty to access all the available sites in the active electrode due to their partial rate of movement in the electrolyte [4]. Comparatively, 6 M KOH and 1 M KCl provide higher specific capacitance when compared with 1 M $NaNO_3$ and 1 M Na_2SO_4. The calculated maximum specific capacitance of 94 F g^{-1} was obtained in 6 M KOH. This observed high capacitance may be explained on the basis of ionic conductivity and hydration sphere radii of cations (Na^+, K^+). Generally, the ionic conductivity and mobility of Na^+ ions are lower than the K^+ ions in aqueous solvent which reduces the charge propagation [34]. Similarly, the K^+ (3.31 Å) ions have low radius of hydration sphere than Na^+ ions (3.58 Å) due to the strong interaction of $Na^{\delta+}$–$H_2O^{\delta-}$. Therefore, the Na^+ ions have the difficult to move through the electrode when compared with K^+ ions [11]. In addition, there may be a large number of K^+-free ions near the electrode surface in the KOH electrolyte than KCl, hence more number of ions contributes to charge storage process. Consequently, the size of the Cl^- (190 pm) anion is greater than the OH^- (133 pm) ion which further enhances the specific capacitance in KOH electrolyte [11]. In contrast, the size of the sulfate (258 pm) anion is bigger than the NO_3^- (179 pm) anion, which may lead to the reduction of Na^+ ions mobility and finally reduces the specific capacitance of Mn_3O_4 electrode. Overall, the charge storage mechanism of this manganese-based electrodes are mainly due to the intercalation and deintercalation of cation (Na^+, K^+) during reduction and oxidation reaction and the adsorption of cations in electrolyte on the surface of the electrode [7, 44]. The observed specific capacitance values are comparatively high when compared with the literature values especially, 14 F g^{-1} at 5 mV s^{-1} in 0.5 M K_2SO_4 reported by Ghodbane et al. [45]. Especially, Komaba et al. reported that the specific capacitance of Mn_3O_4 electrode depends on the ball milling treatment (specific capacitance of Mn_3O_4 before and after milling as approximately less than 8 and 35 F g^{-1}, respectively) and the potential window (the maximum specific capacitance (<70 F g^{-1}) obtained when the potential window is in the range of −0.1 to 0.9 V and also the minimum specific capacitance (<20 F g^{-1}) obtained when the potential window is −0.3 to 0.7 V at a scan rate of 10 mV s^{-1} in 1 M Na_2SO_4 electrolyte [30]). However, the obtained specific capacitance value is lower than the reported Mn_3O_4 composites such as Mn_3O_4/CNT [32], MCMB/Mn_3O_4 [33], Mn_3O_4/worm-like mesoporous carbon [16], and Mn_3O_4/graphene [34] composites which give a higher capacitance value of 143, 178, 266, and 256 F g^{-1} in 0.5 M Na_2SO_4 at a scan rate of 50 mV s^{-1}, 1 M $LiPF_6$ (EC + DMC) at a current rate of 330 mA g^{-1}, 6 M KOH at a scan rate of 1 mV s^{-1}, and 6 M KOH at a scan rate of 5 mV s^{-1}, respectively. This observed low capacitance may be due to the less crystallinity of the Mn_3O_4 nanoparticles which inferred from XRD and Raman

spectrum. It is well known that the specific capacitance of the materials is very high when the materials having high crystallinity, because it enhances the ionic mobility of the charge carriers [7, 44].

3.2.2 Electrochemical impedance spectral analysis

In order to substantiate the CV results, the electrochemical impedance spectroscopy (EIS) analysis was carried out for Mn_3O_4 at different electrolytes of 1 M $NaNO_3$, 1 M Na_2SO_4, 6 M KOH, and 1 M KCl at open circuit potential in the frequency range of 0.01 Hz to 10^5 Hz. The typical Nyquist plot of Mn_3O_4 electrodes are shown in Fig. 5. At high-frequency region, the intersection made on the horizontal axis of the Nyquist plot reveals the solution resistance (R_s). At high-to-medium frequency region, one depressed semicircle was observed, which is related with surface property of the Mn_3O_4 electrode, corresponding to the charge transfer resistance at electrode/electrolyte interface. In addition, at low-frequency region the spike was found, which indicates the characteristic behavior of supercapacitors. The spike represents the Warburg impedance (W) of the electrode, i.e., the diffusive resistance of ions SO_4^{2-}, NO_3^-, Cl^-, and OH^- into electrode [4, 14]. The phase angle of spike greater than 45° for all electrolytes indicates the electrochemical behavior of Mn_3O_4. Comparing all the electrolytes, the electrolyte 6 M KOH (1.197 Ω) has lower solution resistance than other electrolytes such as 1 M KCl (2.046 Ω), 1 M $NaNO_3$ (2.694 Ω), and 1 M Na_2SO_4 (2.839 Ω) electrolytes.

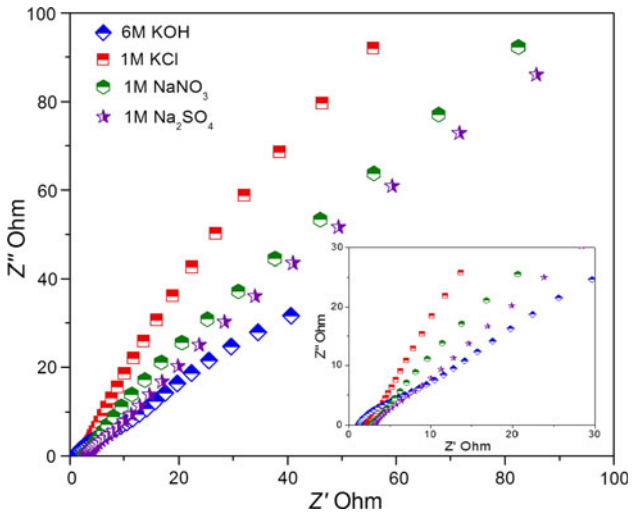

Fig. 5 Nyquist plot of Mn_3O_4 electrode in various electrolytes

3.2.3 Galvanostatic charge–discharge analysis

The galvanostatic charge–discharge analyses of Mn_3O_4 carried out in all the electrolytes at different current densities such as 0.5, 1, 3, and 5 mA cm^{-2} and are shown in Fig. 6. It can be seen that a potential or IR drop was found at early discharging time which may be due to the internal

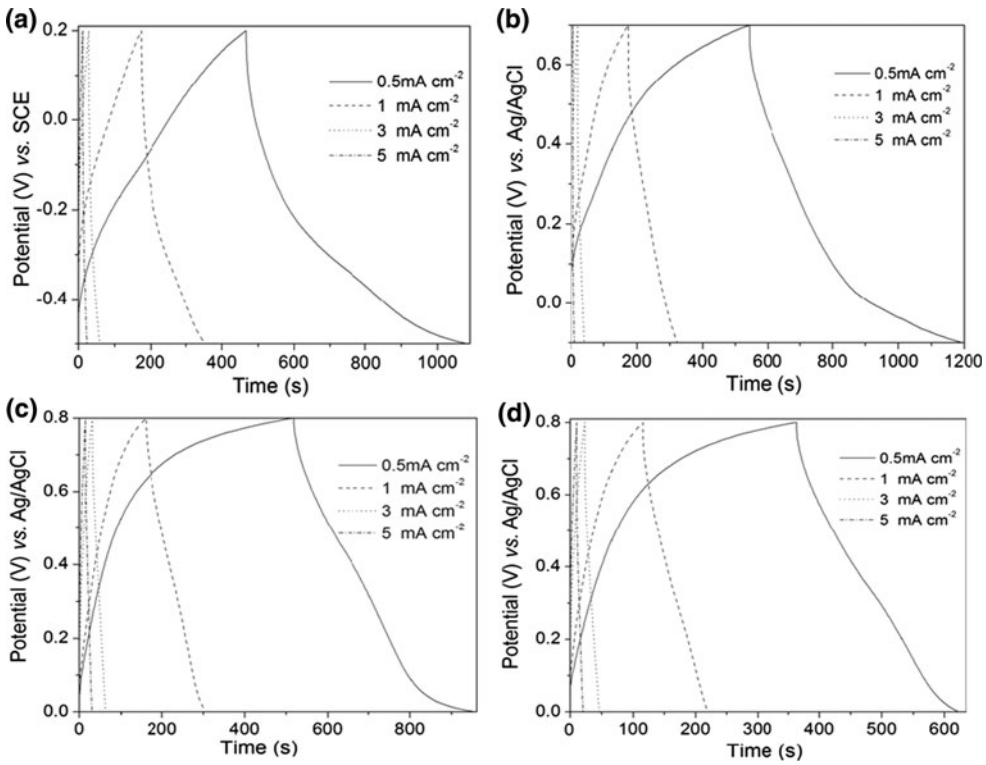

Fig. 6 Galvanostatic charge–discharge curve of Mn_3O_4 electrode in **a** 6 M KOH, **b** 1 M KCl, **c** 1 M $NaNO_3$, and **d** 1 M Na_2SO_4 electrolytes

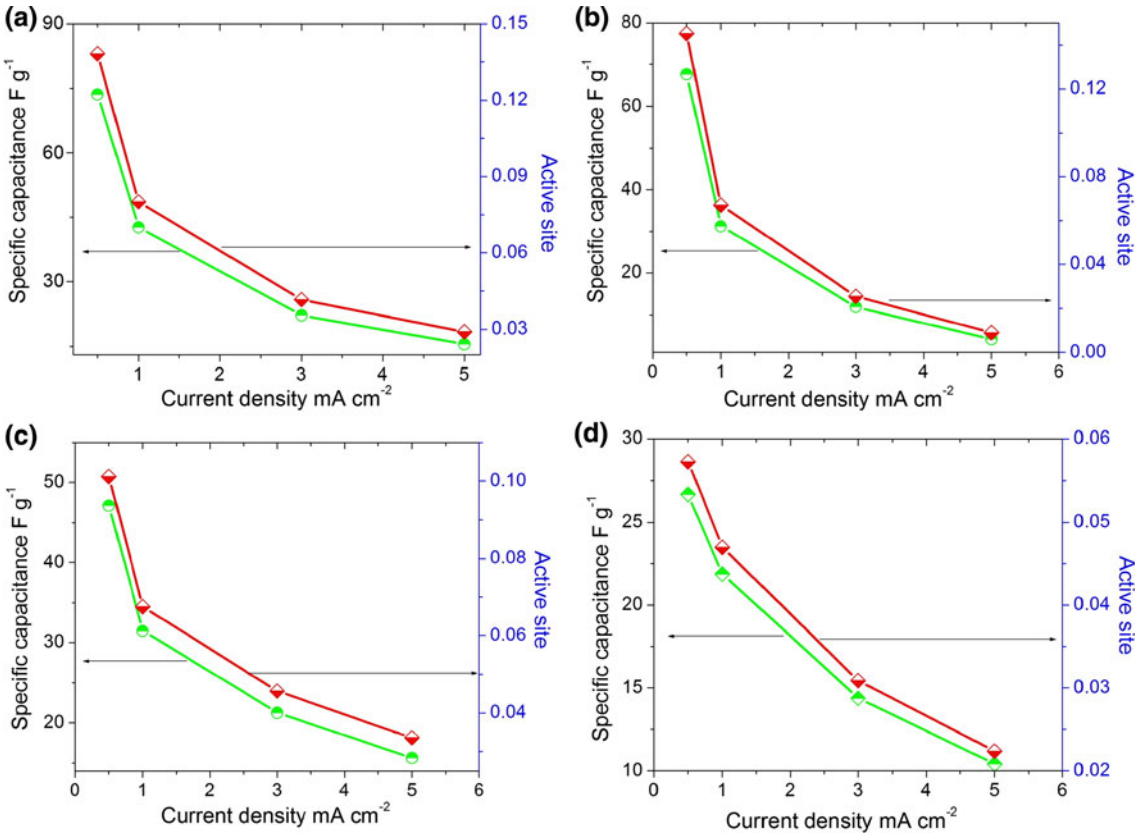

Fig. 7 Specific capacitance and active site variation as a function current density in various aqueous electrolytes such as **a** 6 M KOH, **b** 1 M KCl, **c** 1 M $NaNO_3$, and **d** 1 M Na_2SO_4

resistance of electrode material. It can be related to the contact resistance between the electrode and electrolyte, solution resistance of electrolyte, and charge transfer resistance. The internal resistance of the electrode material increases with increase in current density [46]. The observed symmetric manners of the charge–discharge curves indicate the electrochemical reversibility of Mn_3O_4 electrode. The maximum discharge capacitance is obtained (74 F g^{-1}) at current density of 0.5 mA cm^{-2} in 6 M KOH electrolyte which is comparable to the specific capacitance calculated from CV curve. Figure 7a–d shows the variation of discharge capacitance and active sites with different current density in all the electrolytes. It evidences that the electrode has higher specific capacitance and higher number of active sites at low-current density and vice versa, i.e., lower specific capacitance and active sites at higher current density in all electrolytes. It may be due to the fact that ions completely diffuse into the electrode and utilize all the active sites in electrode at low-current density. Therefore, the specific capacitance and active sites are high. Similarly, at higher current density, the ions have time constraint to utilize all the active sites in electrode. Therefore, the specific capacitance and active sites are low [47].

The cyclic stability of the electrode material is important for supercapacitor applications. In order to find the cyclic stability of the Mn_3O_4 electrode material, the galvanostatic charge–discharge cycle was carried out in all electrolytes at a current density of 5 mA cm^{-2} up to 500 cycles. Figure 8a–d shows the variation of charge and discharge capacitance, and coulombic efficiency with cycle number of Mn_3O_4 electrode in all the electrolytes. The first 10 charge–discharge cycles is given as an inset of Fig. 8. It can be seen that during cycling, the discharge and charging capacitance of the electrode material was increased significantly. According to the earlier reports, this may be due to the occurrence of morphological or structural changes while extended cycling [18, 22, 45]. The coulombic efficiency of the material was maintained approximately greater than 100 %. Overall, it shows that the Mn_3O_4 is a suitable electrode material for supercapacitor application and its suitable electrolyte is 6 M KOH.

4 Conclusions

Mn_3O_4 nanoparticles were successfully synthesized by microwave-assisted reflux synthesis method within 5 min

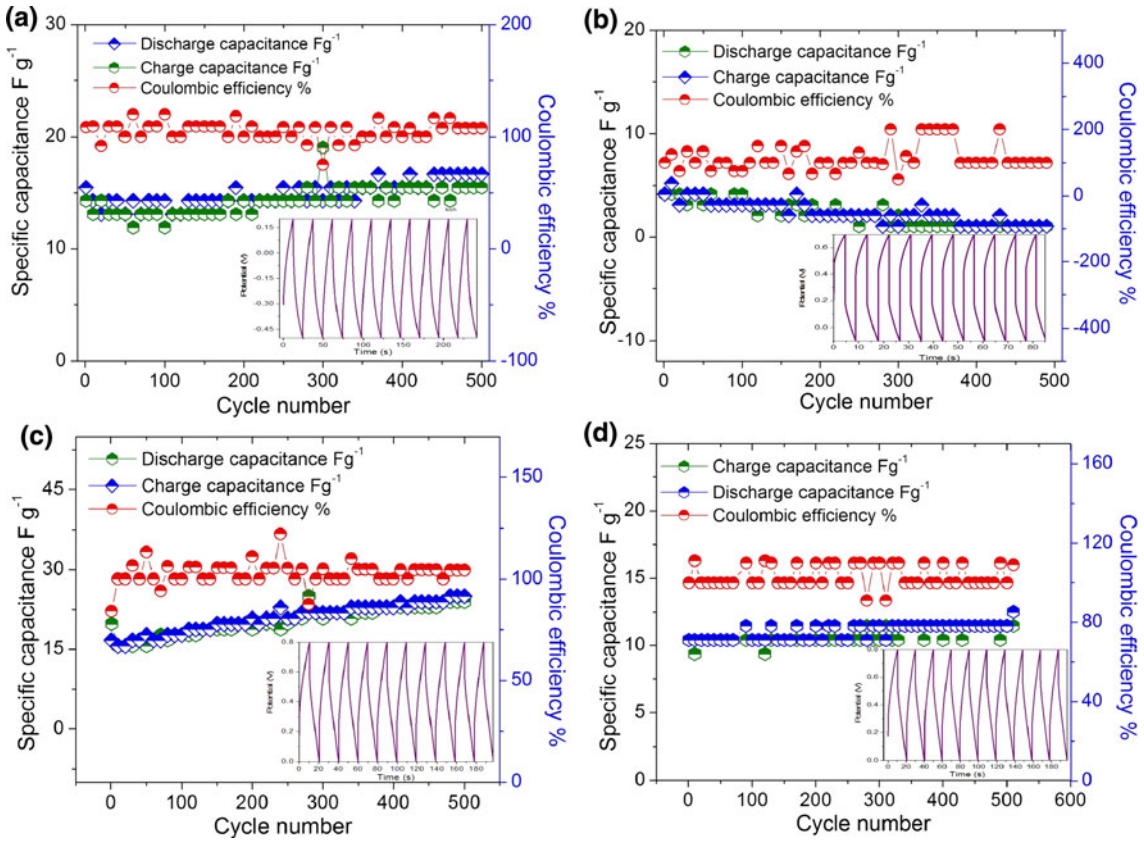

Fig. 8 The effect of cycling on charge, discharge capacitance, and coulombic efficiency of Mn_3O_4 electrodes in **a** 6 M KOH, **b** 1 M KCl, **c** 1 M $NaNO_3$, and **d** 1 M Na_2SO_4 electrolytes, and the inset represents the first 10 cycles of Mn_3O_4 electrode in corresponding electrolytes

without any further heat treatment. The as-prepared Mn_3O_4 samples possess tetragonal structure, and its lattice parameters and grain size were calculated from XRD pattern. FT-IR and Raman analyses confirmed the compound formation and the presence of the functional groups in as-prepared Mn_3O_4 samples. The TEM result reveals the presence of smaller particle size (50 nm). The electrochemical properties of Mn_3O_4 electrode were investigated in various aqueous electrolytes. The CV results reveal that the Mn_3O_4 electrode possesses higher specific capacitance (94 F g^{-1}) in 6 M KOH electrolyte. Therefore, 6 M KOH electrolyte may be adopted as electrolyte for better capacitance performances. The electrochemical impedance analysis and galvanostatic charge–discharge analysis further confirm that the Mn_3O_4 electrode has lower internal resistance and higher capacitance in 6 M KOH electrolyte than other electrolytes. The long-term cycle stability Mn_3O_4 electrode reveals that the prepared sample is a suitable electrode material for supercapacitor applications.

References

1. Zhao X, Sanchez BM, Dobson PJ, Grant PS (2011) Nanoscale 3:839
2. Conway BE (1999) Electrochemical supercapacitors. Kluwer-Plenum, New York
3. Devadas A, Baranton S, Napporn TW, Coutanceau C (2011) J Power Sources 196:4044
4. Meher SK, Justin P, Rao GR (2011) Appl Mater Interfaces 3:2063
5. Yuan YF, Xia XH, Wu JB, Huang XH, Pei YB, Yang JL, Guo SY (2011) Electrochem Commun 13:1123
6. Zheng FL, Li GR, Ou YN, Wang ZL, Su CY, Tong YX (2010) Chem Commun 46:5021
7. Kalai Selvan R, Perelshtein I, Perkas N, Gedanken A (2008) J Phys Chem C 112:1825
8. Zhang Y, Li GY, Lv Y, Wang LZ, Zhang AQ, Song YH, Huang BL (2011) Int J Hydrogen Energy 36:11760
9. Xing S, Zhou Z, Ma Z, Wu Y (2011) Mater Lett 65:517
10. Hu CC, Hung CY, Chang KH, Yang YL (2011) J Power Sources 196:847
11. Reddy RN, Reddy RG (2003) J Power Sources 124:330
12. Xu MW, Jia W, Bao SJ, Su Z, Dong B (2010) Electrochim Acta 55:5117
13. Ding KQ (2008) J Chin Chem Soc 55:543
14. Xia H, Xiao W, Lai MO, Lu L (2009) Nanoscale Res Lett 4: 1035
15. Hao X, Zhao J, Li Y, Zhao Y, Ma D, Li L (2011) Colloid Surf Physicochem Eng Aspect 374:42
16. Zhou T, Mo S, Zhou S, Zou W, Liu Y, Yuan D (2011) J Mater Sci 46:3337
17. Jiang H, Zhao T, Yan C, Ma J, Li C (2010) Nanoscale 2:2195
18. Dubal DP, Dhawale DS, Salunkhe RR, Lokhande CD (2010) J Electroanal Chem 647:60

19. Dubal DP, Dhawale DS, Salunkhe RR, Fulari VJ, Lokhande CD (2010) J Alloys Compd 497:166
20. Li Y, Tan H, Yang XY, Goris B, Verbeeck J, Bals S, Colson P, Cloots R, Tendeloo GV, Su BL (2011) Small 4:475
21. Gao W, Ye S, Shao M (2011) J Phys Chem Solids 72:1027
22. Dubal DP, Dhawale DS, Salunkhe RR, Lokhande CD (2010) J Alloys Compd 496:370
23. Ozkaya T, Baykal A, Kavas H, Kőseoğlu Y, Toprak MS (2008) Phys B 403:3760
24. Baykal A, Kavas H, Durmuş Z, Demir M, Kazan S, Topkaya R, Toprak MS (2010) Cent Eur J Chem 8(3):633
25. Zhang W, Yang Z, Liu Y, Tang S, Han X, Chen M (2004) J Cryst Growth 263:394
26. Bilecka I, Niederberger M (2010) Nanoscale 2:1358
27. Apte SK, Naik SD, Sonawane RS, Kale BB, Pavaskar Neela, Mandale AB, Das BK (2006) Mater Res Bull 41:647
28. Berthelin CB, Stuerga D (2005) J Mater Sci 40:253
29. Malinger KA, Ding YS, Sithambaram S, Espinal L, Gomez S, Suib SL (2006) J Catal 239:290
30. Komaba S, Tsuchikawa T, Ogata A, Yabuuchi N, Nakagawa D, Tomita M (2012) Electrochim Acta 59:455
31. Devaraj S, Munichandraiah (2008) J Phys Chem C 112:4406
32. Cui X, Hu F, Wei W, Chen W (2011) Carbon 49:1225
33. Wang H, Li Z, Yang J, Li Q, Zhong X (2009) J Power Sources 194:1218
34. Wang B, Park J, Wang C, Ahn H, Wang G (2010) Electrochim Acta 55:6812
35. Dubal DP, Dhawale DS, Salunkhe RR, Pawar SM, Lokhande CD (2010) Appl Surf Sci 256:4411
36. Gibot P, Laffont L (2007) J Solid State Chem 180:695
37. Patra CR, Gedanken A (2004) New J Chem 28:1060
38. Wang H, Zhu JJ, Zhu JM, Liao XH, Xu S, Ding T, Chen HY (2002) Phys Chem Chem Phys 4:3794
39. Senthilkumar B, Thenamirtham P, Kalai Selvan R (2011) Appl Surf Sci 257:9063
40. Anilkumar M, Ravi V (2005) Mater Res Bull 40:605
41. Sekar C, Kalai Selvan R, Senthilkumar ST, Senthilkumar B, Sanjeeviraja C (2012) Powder Technol 98:215
42. Yang LX, Zhu YJ, Tong H, Wang WW, Cheng GF (2006) J Solid State Chem 179:1225
43. Zuo J, Xu C, Liu Y, Qian Y (1998) Nanostruct Mater 10:1331
44. Sharma RK, Oh HS, Shul YG, Kim H (2008) Phys B 403:1763
45. Ghodbane O, Pascal JL, Fraisse B, Favier F (2010) Appl Mater Interfaces 2:3493
46. Zhang J, Jiang J, Zhao XS (2011) J Phys Chem C 115:6448
47. Xu J, Gao L, Cao J, Wang W, Chen Z (2010) Electrochim Acta 56:732